Qing Wang, Deng-Guang Yu*, Sun-Yi Zhou, Chen Li and Min Zhao*

Electrospun amorphous medicated nanocomposites fabricated using a Teflon-based concentric spinneret

https://doi.org/10.1515/epoly-2017-0110
Received June 6, 2017; accepted July 13, 2017; previously published online August 18, 2017

Abstract: Facile methods to improve the dissolution rate of poorly water-soluble drugs are highly sought after. In this study, a modified coaxial electrospinning process was exploited to create medicated amorphous nanocomposites, an approach characterized by the application of a Teflon-coated coaxial spinneret. The hydrophilic polymer hydroxypropyl methylcellulose and the active ingredient tamoxifen citrate (TAM) were selected as the drug carrier and model drug, respectively. Their electrospun nanocomposites showed linear morphology with the drug presented in an amorphous state. The loaded cargoes could be released from the nanocomposites simultaneously when they were placed in the dissolution media, showing faster dissolution rates than their counterparts (physical mixtures). Based on the reasonable application of the polymeric carrier, the reported protocols not only provided an approach to enhance the dissolution of poorly water-soluble drugs, but also exhibited a method to facilitate the implementation of coaxial electrospinning.

Keywords: modified coaxial electrospinning; nanocomposite; polymeric composite; poorly water-soluble drug; Teflon.

1 Introduction

Solid dispersion (SD) represents one of the most popular technologies for developing oral solid dosage forms of poorly water-soluble active pharmaceutical ingredients (1). Medicated polymer-based composites are advanced SDs and are attracting considerable interest in the fields of biomedicine and polymers (2–4). During the past several decades, the number of poorly water-soluble drugs continued increasing with the progress of organic chemistry and biomedical engineering (5). Correspondingly, more methods are being introduced into this field for the effective delivery of these drugs. One of the key elements for the success of new methods is the reasonable selection and application of drug carriers. The different kinds of drug carriers include polymers, phospholipids, surfactants, polysaccharides and proteins; moreover, pharmaceutical hydrophilic polymers are the most suitable candidates for SDs. These polymers often have good processability by a series of methods. They have an amorphous physical state and can effectively retard the recrystallization of drugs when they are transferred into amorphous composites (6). One example is polyvinylpyrrolidone (PVP), broadly reported to create drug-loaded composites to improve the dissolution rates of poorly water-soluble drugs (7–10). However, PVP is a synthetic polymer. Many natural polymer products, such as derivatives of cellulose, may have good applications for developing amorphous composites because of their biocompatibility, abundant supply and low cost.

Medicated nanofibers consisting of a guest drug and a host polymer are often prepared using a single-fluid blending electrospinning process (11, 12). Within these monolithic nanofibers, drug molecules are homogeneously distributed into the polymeric matrices, suggesting an amorphous drug-loaded nanocomposite. A traditional single-fluid electrospinning system consists of four elements: a power supply, a syringe pump, a spinneret and a collector. Among them, the spinneret is the most important element, by which different types of electrospinning processes are categorized (such as coaxial electrospinning, side-by-side electrospinning and tri-axial electrospinning) (13–17). Thus far, nearly all the spinnerets (whether single tube, coaxial capillaries, or side-by-side parallel capillaries) are produced using metal tubes because electrical energy is readily transferred into the working fluid by metal materials. However, some of the

***Corresponding authors: Deng-Guang Yu,** School of Materials Science and Engineering, University of Shanghai for Science and Technology, Shanghai, China, e-mail: ydg017@usst.edu.cn; and **Min Zhao,** School of Pharmacy, Queen's University Belfast, Belfast, UK, e-mail: m.zhao@qub.ac.uk
Qing Wang and Sun-Yi Zhou: School of Materials Science and Engineering, University of Shanghai for Science and Technology, Shanghai, China
Chen Li: Institute of Biotechnology, Shanxi University, Taiyuan, Shanxi, China

latest investigations disclosed that the modification of spinnerets by polymeric materials can effectively facilitate the implementation of this advanced technology (18–22).

Based on the aforementioned information, the present research exhibited two ways for the effective application of polymers for advanced technology. One is for the SD technique, wherein hydroxypropyl methylcellulose (HPMC) was exploited to create an amorphous composite-based nano SD for an anticancer model drug called tamoxifen citrate (TAM). The other method is for the easy and smooth implementation of advanced fiber-forming nanotechnology, i.e. modified coaxial electrospinning, which is derived from traditional coaxial electrospinning. In the modified coaxial processes, liquids without electrospinnability can be utilized as sheath working fluids. Given that electrospinnable polymeric solutions are very limited whereas numerous unspinnable liquids (such as suspensions, emulsions, solvents and solutions containing minimal chemical molecules) are available, the modified coaxial process can significantly expand the capability of electrospinning in generating novel nanomaterials (11, 23).

2 Materials and methods

2.1 Materials

Tamoxifen citrate (TAM, content >99%) was provided by Wuhan Beika Biological Pharmaceutical Co. Ltd. (Hubei, China). Hydroxypropyl methylcellulose (HPMC, 5 mPas) was obtained from Shandong Nice Chemical Co. Ltd. (Jinan, China). Methylene blue, anhydrous ethanol and dichloromethane were purchased from Shanghai Chemical Reagents Co. Ltd. (Shanghai, China). All chemicals were analytical reagents, and water was double distilled prior to use.

2.2 Modified coaxial electrospinning

All preparations were conducted using a modified coaxial electrospinning process, which was characterized by a homemade Teflon-coated coaxial spinneret (20). A ZGF60 kV/2 mA power supply (Wuhan Huatian Corp., Wuhan, China), two KDS100 syringe pumps (Cole-Parmer, Vernon Hills, IL, USA), and a cardboard wrapped with aluminum foil were utilized to set up the electrospinning system.

Based on previous experiments, an electrospinnable solution consisting of 13 (w/v)% of HPMC and 2 (w/v)% TAM in a mixture of ethanol and dichloromethane (1:2, v:v) was used as the core fluid. (For preliminary tests to determine the experimental conditions, 5 μg/ml methylene blue was added to the core fluid.) A pure solvent mixture containing ethanol and dichloromethane in a volume ratio of 1:2 was utilized as the sheath fluid. Under a fixed-core flow rate of 1.0 ml/h, five different types of nanofibers were fabricated under a varied sheath fluid flow rate, referred to as F1, F2, F3, F4, and F5 for a rate of 0.1, 0.2, 0.3, 0.4, and 0.5 ml/h, respectively. The ambient conditions included a temperature of 21 ± 4°C and a relative humidity of 57 ± 5%. The applied voltage and fiber-collected distance were fixed at 15 kV and 20 cm for all the preparations. The coaxial processes were recorded using a PowerShot A640 Digital Camera (Tokyo, Japan). A physical mixture (PM) consisting of 6.5 g HPMC and 1 g TAM powders was prepared as a control.

2.3 Morphology

The morphology of the fibers was examined using a scanning electron microscope (SEM, FEI Quanta 200 FEG ESEM instrument). Each specimen was fixed with conductive double-sided carbon adhesive tape and were gold sputter-coated under a nitrogen atmosphere to render them electrically conductive. The average fiber diameter was determined by measuring their sizes in SEM images at more than 100 different places using the ImageJ Software (National Institutes of Health, Bethesda, MD, USA). The topographies of raw HPMC and TAM were observed under cross-polarized light using an XP-700 polarized optical microscope (OM, Shanghai Changfang Optical Instrument, Shanghai, China).

2.4 Physical forms and compatibility

X-ray powder diffraction (XRD) patterns were recorded using a Bruker X-ray Powder Diffractometer Bruker-AXS with Cu Kα radiation (Karlsruhe, Germany). The applied voltage was 40 kV, while the current was 30 mA. The untreated materials and the fibrous samples were analyzed between 2θ angles from 5° to 60°. Attenuated total reflectance (ATR)-Fourier transform infrared (FTIR) analysis was implemented on a Spectrum 100 FTIR Spectrometer (PerkinElmer, Billerica, MA, USA). Spectra were recorded over the range of 700–4000 cm^{-1} at a resolution of 2 cm^{-1}. Approximately 5 mg of the materials

were placed directly on the diamond window for spectra acquisition.

2.5 Fast dissolution performance

In vitro dissolution tests were performed using a RCZ-8A dissolution apparatus (Tianjin University Radio Factory, Tianjin, China). Samples equivalent to 40 mg of TAM (i.e. 0.3 g medicated fibers or physical mixture) were placed into the dissolution cells, where the dissolution medium (900 ml physiological saline) was kept at a constant temperature of 37 ± 1°C. The paddle frequency was always held at 50 rpm. A UV-vis spectrophotometer (UV-2102PC, Unico Instrument Co. Ltd., Shanghai, China) was used to measure the concentration of dissolved TAM at a wavelength of $\lambda = 278$ nm. The percentage of dissolution could be readily calculated based on the calibration curve of TAM. The experiments were carried out 6 times, and the accumulative release amounts reported as mean values were plotted as a function of time (T, min).

3 Results and discussion

3.1 Modified coaxial process characterized by Teflon-coated spinneret

The modified coaxial electrospinning process, an upgraded version of the traditional coaxial electrospinning, is characterized by the use of unspinnable liquids as the sheath working fluids (23–25). Detailed observations of modified coaxial electrospinning processes under a series of sheath fluid flow rates are shown in Figure 1. Figure 1A–D illustrates that the larger the sheath fluid flow rates were, the smaller were the volumes of the Taylor cones. These fluids were pumped out similarly from the coaxial exit of the Teflon-based spinneret; thus, their Taylor cones possessed the same bottom size (i.e. 2.0 mm), but their heights gradually decreased from 2.3 mm to 2.0, 1.8 and 1.3 mm, for a sheath fluid flow rate of 0.1, 0.2, 0.3 and 0.4 ml/h, respectively. According to the height and bottom size of their Taylor cones, the semi-vertical angle of the Taylor cone (α), i.e. the sharpness of the hyperboloid, can be calculated. For forming fibers F1–F4, the angles were gradually increased from 26° to 30°, 34° and 50°, respectively. The larger the sheath fluid flow rates were, the larger the angle at which the straight jets were emitted, suggesting that the sheath pure solvent could facilitate the electrospinning processes. All the Taylor cones indicated that a slight diffusion of methylene blue from the core solution to the sheath solvent occurred during the electrospinning processes.

Figure 1E shows the coaxial processes under a sheath flow rate of 0.5 ml/h, which consisted of three typical procedures of a standard electrospinning process, i.e. the Taylor cone followed by a straight fluid jet (with a length of 5.4 mm) and followed by a highly frequent bending and whipping region with enlarged coils. These enlarged coils had bright dots on the lines, suggesting an insufficient drawing of the fluid jets. Compared to other Taylor cones, this one was even flatter with an estimated height of 0.9 mm. Figure 1F shows the collection of monolithic

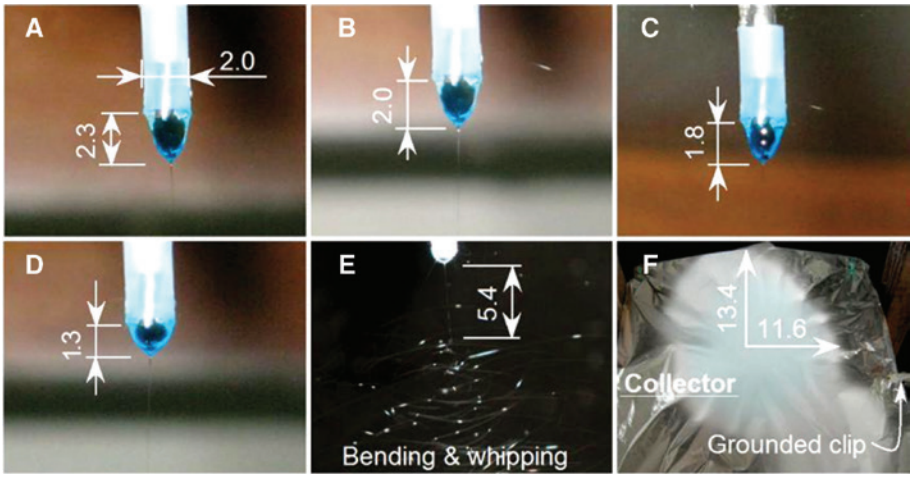

Figure 1: Observations of the modified coaxial electrospinning processes. Images of Taylor cones under the varied sheath fluid flow rate (ml/h): (A) 0.1; (B) 0.2; (C) 0.3; (D) 0.4; (E) the whole electrospinning process with a sheath fluid flow rate of 0.5 ml/h; and (F) the randomly assembled nanofiber mat of F1 on the fiber collector.

nanofiber F1, which assembled into a non-woven mat with a length of 13.4 × 2 mm and a width of 11.6 × 2 mm. The collector was facilely grounded by an alligator clipper. The other collected nanofiber mats (F2–F5) exhibited a similar condition.

3.2 Morphology of prepared composite nanofibers

The SEM images of the amorphous nanofibers collected under different sheath fluid flow rates are exhibited in Figure 2. Figure 2A–D shows nanofibers created under sheath fluid flow rates of 0.1, 0.2, 0.3 and 0.4 ml/h, respectively. Each nanofiber has a linear morphology with a smooth surface, as indicated by their upper-right insets. Their diameters were estimated (see Figure 2G–J) and these nanofibers have average diameters (nm) of 760 ± 120 (F1), 610 ± 110 (F2), 450 ± 80 (F3) and 220 ± 50 (F4), respectively.

However, beads-on-a-string morphology appeared when the sheath fluid flow rate was further increased to 0.5 ml/h (Figure 2E). This effect could be forecast by the observations of the coaxial electrospinning processes in Figure 1E. Although these nanofibers further decreased in size, their beads had a larger size, resulting in a non-uniform nanostructure. This outcome is unfavorable for their use as drug delivery materials. Figure 2F consists of the images of raw TAM particles that were in a prismatic topography.

3.3 Influence of sheath fluid flow rate on coaxial processes and formation of nanofibers

To further disclose the influence of sheath fluid flow rate on the coaxial processes and on the formation of nanofibers, the height of the Taylor cone (*H*) and the diameter of fiber (*D*) were expressed as the functions of sheath-to-core

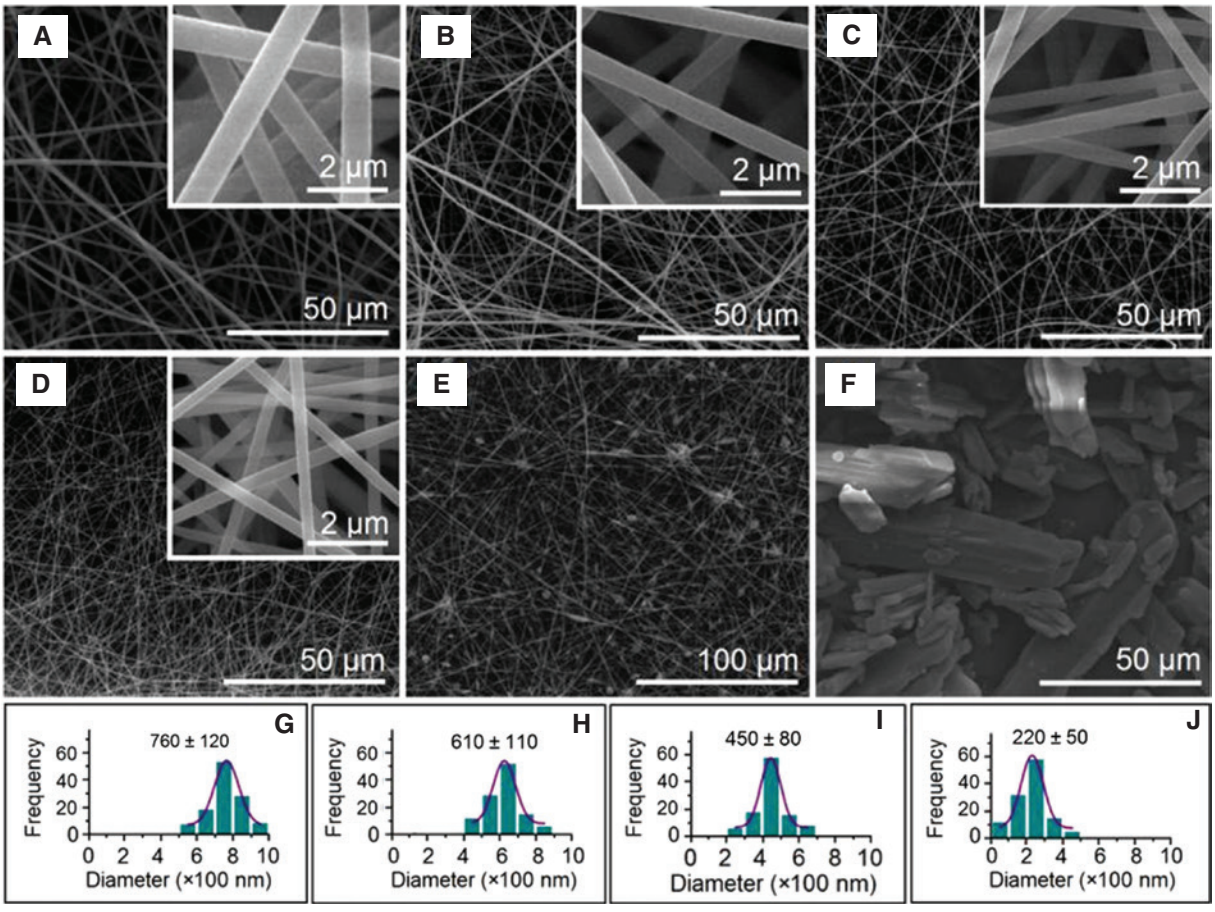

Figure 2: The SEM images of amorphous nanofibers collected under different sheath fluid flow rates (ml/h): (A) 0.1; (B) 0.2; (C) 0.3; (D) 0.4 (insets show enlarged SEM images); (E) 0.5; (F) SEM images of raw TAM particles; and (G)–(J) show the statistical data of the diameters of nanofibers F1–F4, respectively.

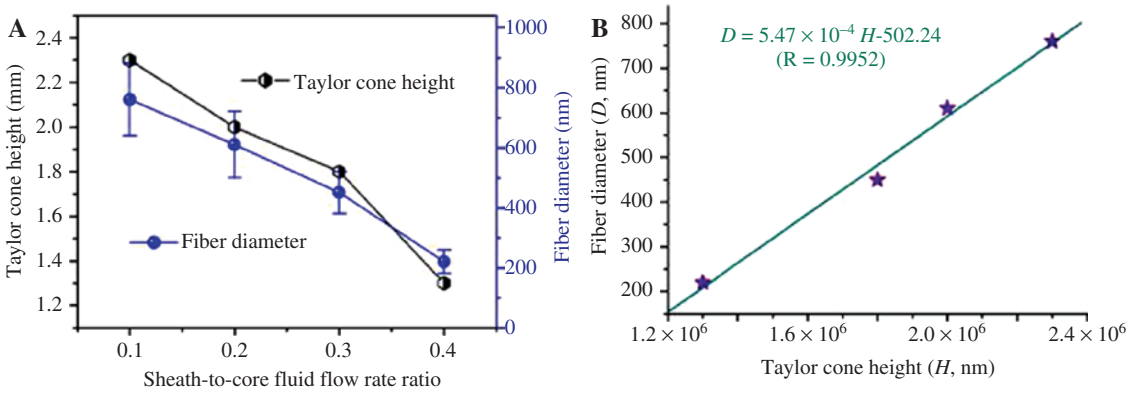

Figure 3: Influence of sheath fluid flow rates on the coaxial processes. (A) The change trend of the Taylor cone height and fiber diameters with the increase of the sheath-to-core fluid rate ratio; (B) the linear relationship between the Taylor cone height and the fiber diameter.

fluid flow rate ratio (F) in Figure 3A. The Taylor cone height and fiber diameter showed a similar trend of becoming increasingly smaller as the ratio gradually increased. The regressed linear equations were $H = 2.65–3.2F$ ($|R| = 0.9829$) and $D = 955–1780F$ ($|R| = 0.9843$). Their correlation coefficients suggested a near linear relationship between the Taylor cone height and fiber diameter with the sheath-to-core fluid flow rate ratio.

However, a better linear relationship was found when the fiber diameter was built as a function of the Taylor cone height, as shown in Figure 3B. The linear relationship was $D = 5.47 \times 10^{-4}$ H-502.24, which has a correlation coefficient of 0.9952. This relationship was very useful for manipulating the coaxial electrospinning processes. According to these results, many other methods may be attempted for reducing nanofiber diameters through downsizing the Taylor cone, such as using a capillary with a small nozzle as the spinneret, increasing the field strength to decrease the size of the Taylor cone, and elevating the conductivity of working fluids (26–28).

3.4 Physical state of components and their compatibility within nanofibers

The XRD patterns of the raw materials (TAM and HPMC), their composite fibers F4 and their PM are shown in Figure 4A. As expected, the drug TAM and its PM with HPMC powders show sharp peaks in their XRD patterns, suggesting the presence of crystal materials due to the TAM particles. By contrast, both HPMC and fiber F4 patterns lack sharp peaks, indicating that they were amorphous materials (fibers F1, F2, and F3 with similar patterns as fibers F4 and are not included in Figure 4A). To further observe the morphology of the raw materials, polarized OM was utilized to record their images.

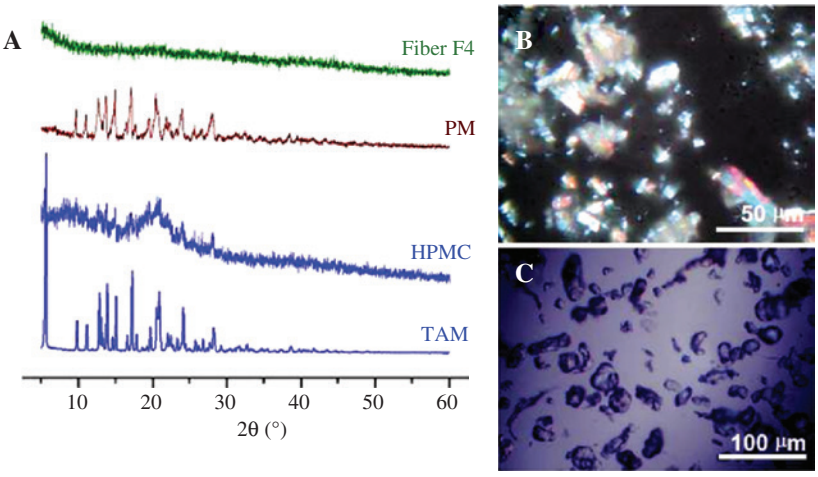

Figure 4: Physical forms of the raw materials and the electrospun amorphous composites. (A) Their XRD patterns; (B) polarized OM morphology of TAM drug particles; (C) polarized OM morphology of HPMC particles.

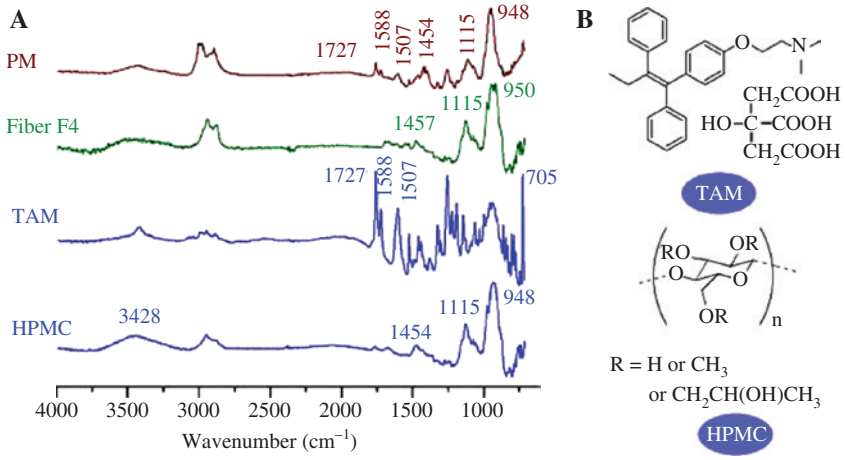

Figure 5: Compatibility between TAM and HPMC within their electrospun amorphous composites. (A) Their ATR-FTIR spectra; (B) molecular formulas of TAM and HPMC.

Figure 4B displays a typical image of the raw TAM particles. The bright colors (including red, blue and green), which should be the results of their crystal surfaces in the TAM particles, were likewise demonstrated by acetaminophen particles (20). By contrast, the HPMC raw particles show a monotonous blue background color, reflecting the amorphous property of HPMC powders. These results demonstrated that the electrospinning process could be exploited to prepare medicated amorphous nanocomposites for the poorly water-soluble crystalline drugs, which is a long-existing concern in the field of pharmaceutics.

The ATR-FTIR spectra of the raw materials (TAM and HPMC) are exhibited in Figure 5A. Owing to the presence of benzene rings, TAM spectra have the typical peaks of 1727, 1588, 1507 and 705 cm^{-1}. However, these typical peaks disappeared from the spectra of fibers F4 but could be discerned in the spectra of PM. This difference reflects the different states of TAM in the PM and electrospun nanofibers. The presence of typical spectra of benzene rings in the PM spectra suggested the existence of TAM crystalline particles, whereas their disappearance from the spectra of fibers F4 demonstrated that no TAM crystalline particles were present in the electrospun fibers. Similar results were achieved for fibers F1, F2 and F3.

These results concurred with those observed in the XRD tests, demonstrating the good compatibility between TAM and HPMC molecules. TAM and HPMC molecular formulas are shown in Figure 5B. Tamoxifen is insoluble in water. Its citrate derivative, i.e. TAM, has improved water solubility, but still belongs to the Class II poorly water-soluble drugs (29, 30). However, the incorporation of carboxyls and hydroxyls into TAM molecules allows them to easily form hydrogen bonds with HPMC molecules (31). HPMC molecules have numerous hydroxyls that can act as proton donors for the formation of hydrogen bonds with TAM molecules, which in turn can act as proton receptors. These favorable secondary interactions not only increase the compatibility of the components within the electrospun nanofibers, but should also support the stability of amorphous nanocomposites by retarding the solid phase separations within them.

3.5 Functional performance of amorphous medicated nanocomposites

The drug release profiles from the different kinds of electrospun medicated nanofibers and the PM are shown in Figure 6A (full time period) and B (the initial 5 min). Clearly, all the electrospun nanofibers could free their cargoes within 15 min, much faster than their counterpart, the PM of TAM and HPMC particles (Figure 6A). Traditional TAM tablets are often prepared from a physical mixture of raw drug and drug carrier powders by direct compression methods. The release profile of PM, a direct reflection of commercial TAM tablets, showed an unfavorable release over 4 h with a long-time period tailing off drug release. For the four types of electrospun amorphous nanofibers from the Teflon-coated spinneret, fibers F3 and F4 were able to exhaust all the contained drugs within 2 min, faster than the PM in double orders of magnitude. Meanwhile, fibers F3 and F4 were twice as fast as fibers F1 and F2, which released about 70% of their contained drugs at the initial 2 min (Figure 6B).

Methods to enhance drug dissolution rates are highly sought after, particularly for drugs with poorly

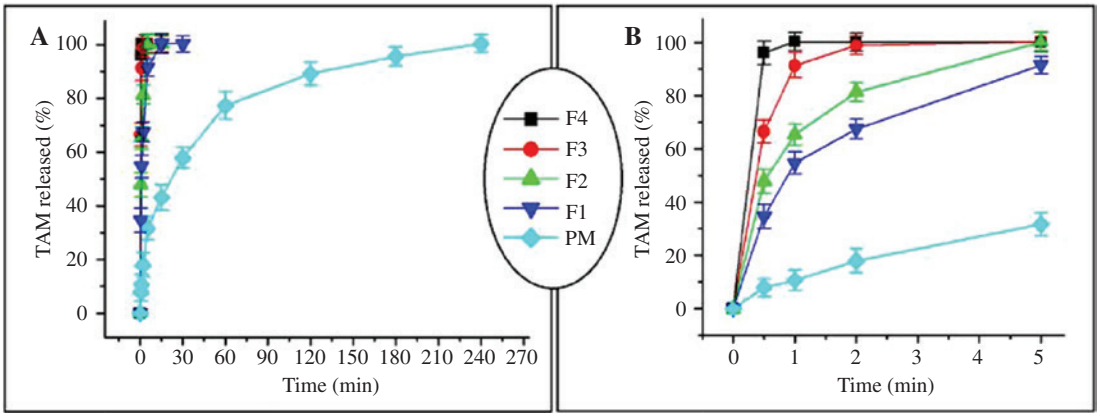

Figure 6: Drug fast release functional performance of the amorphous composites and physical mixtures: (A) full time period; (B) initial 5 min.

water-soluble properties. Generally, these methods can be guided by the Noyes-Whitney equation, by which the dissolution rate (dq/dt) is described as follows (32):

$$dq/dt = (s \times d/\delta) \times (c_0 - x/v),$$

where q is the amount of drug released from the solid dosage forms, t is the drug release time, s is the effective drug release surface area, d is the diffusion coefficient of the drug from the dosage form to the bulk dissolution media, δ is the effective diffusion boundary layer, c_0 is the saturation solubility of the drug, and v is the volume of the dissolution medium. Based on the equation, the drug release rate is directly proportional to the surface area of the dosage forms, which should be a reason why nanotechnologies are very popular in developing new types of drug delivery systems for poorly water-soluble drugs.

The electrospun amorphous composite nanofibers have the following advantages over the PM for enhancing the dissolution rates of poorly water-soluble drugs: (1) They had nanoscale diameters and a 3D assembled manner, thereby providing a huge surface area for drug release. (2) An amorphous drug state of TAM with the HPMC matrices suggests that no lattice energy needed to be overcome during the dissolution processes. A combination of the nanoscale effect and drug physical state alterations resulted in the more rapid release of TAM from HPMC nanofibers than from its PM. The faster release of TAM from F3 and F4 than from F1 and F2 has a close relationship with their relatively small diameters. For example, F4 and F1 had an average diameter of 220 nm and 760 nm, respectively.

For the cylindrical nanofibers, their volume (V) can be roughly calculated according to the equation $V = r^2\pi L$, where r and L are the radius and length of the fiber. The surface area of nanofibers (S) can be calculated according to the equation $S = 2\pi rL$. Based on the same volumes of nanofibers F1 ($V_1 = r_1^2\pi L_1$) and F4 ($V_4 = r_4^2\pi L_4$), the following relationship can be achieved: $r_1^2\pi L_1 = r_4^2\pi L_4$, i.e. $L_4/L_1 = r_1^2/r_4^2$. Thus, the surface area ratio of fibers F4–F1 can be deduced as follows:

$$\begin{aligned} S_4/S_1 &= (2\pi r_4 L_4)/(2\pi r_1 L_1) \\ &= r_4/r_1 \cdot L_4/L_1 \\ &= r_4/r_1 \cdot r_1^2/r_4^2 = r_1/r_4 \\ &= 380/110 = 3.45. \end{aligned}$$

Thus, the reduction of the nanofiber diameters from 760 nm for fibers F1 to 220 nm for fibers F4 resulted in an effective increase of the nanofiber surface area by magnifications of 3.45 times, which, in turn, generated a more than doubled rate of faster TAM release performance.

4 Conclusions

A Teflon-based concentric spinneret was utilized in conducting the modified coaxial electrospinning processes to create monolithic medicated nanofibers. These HPMC-based nanofibers were essentially drug-loaded polymeric nanocomposites, representing a useful method to improve the dissolution rates of poorly water-soluble drugs. The coaxial processes were conducted facilely in a controllable manner with the generated nanofibers having linear morphology and a smooth surface. The drug TAM was present in an amorphous state in the composite fibers and had good compatibility within its carrier HPMC. The electrospun composite nanofibers could free the loaded anti-cancer TAM within 2 min, which is double

the order of magnitude for the corresponding PM of the raw ATM and HPMC particles. The TAM dissolution performance of amorphous nanofibers had a close relationship with their diameters. The smaller the diameter, the faster the release of the drug. These results demonstrated that reasonable applications of polymers not only facilitated the implementation of the advanced coaxial electrospinning technique but also achieved high-quality nanoproducts for medical applications with improved functional performance.

Acknowledgments: The following projects are highly appreciated: the National Natural Science Foundation of China (No. 51373101), the College Student Innovation Project of USST (Nos. SH2016176-2017189-190-191 and XJ2017286), the Natural Science Foundation of Shanxi Province (No. 2015021047) and the Science & Technology Innovation Project in High School of Shanxi Province (No. 2016116).

References

1. Chen L, Okuda T, Lu XY, Chan HK. Amorphous powders for inhalation drug delivery. Adv Drug Delivery Rev. 2016;100:102–15.
2. Suwantong O. Biomedical applications of electrospun polycaprolactone fiber mats. Polym Adv Technol. 2016;27: 1264–73.
3. Agarwal S, Greiner A, Wendorff JH. Functional materials by electrospinning of polymers. Prog Polym Sci. 2013;38(6): 963–91.
4. Yalcinkaya F, Lubasova D. Quantitative evaluation of antibacterial activities of nanoparticles (ZnO, TiO_2, ZnO/TiO_2, SnO_2, CuO, ZrO_2, and $AgNO_3$) incorporated into polyvinyl butyral nanofibers. Polym Adv Technol. 2017;28:137–40.
5. Wu YH, Yu DG, Li JJ, Wang Q, Li HP, Li XY. Medicated multiple-component polymeric nanocomposites fabricated using electrospraying. Polym Polym Compos. 2017;25(1):57–62.
6. Liu ZP, Cui L, Yu DG, Zhao ZX,Chen L. Electrosprayed core-shell solid dispersions of acyclovir fabricated using an epoxy-coated concentric spray head. Int J Nanomed. 2014;2014(9):1967–77.
7. Li C, Yu DG, Williams GR, Wang ZH. Fast-dissolving core-shell composite microparticles of quercetin fabricated using a coaxial electrospray process. PLoS One. 2014;9(3):e92106.
8. Démuth B, Farkas A, Balogh A, Bartosiewicz K, Kállai-Szabó B, Bertels J, Vigh T, Mensch J, Verreck G, Assche IV, Marosi G, Nagy ZK. Lubricant-induced crystallization of itraconazole from tablets made of electrospun amorphous solid dispersion. J Pharm Sci. 2016;105:2982–8.
9. Démuth B, Nagy ZK, Balogh A, Vigh T, Marosi G, Verreck G, Assche V, Brewster ME. Downstream processing of polymer-based amorphous solid dispersions to generate tablet formulations. Int J Pharm. 2015;486(1):268–86.
10. Yang GZ, Li HP, Yang JH, Wan J, Yu DG. Influence of working temperature on the formation of electrospun polymer nanofibers, Nanoscale Res Lett. 2017;12(1):1–10.
11. Wen HF, Yang C, Yu DG, Li XY, Zhang DF. Electrospun zein nanoribbons for treatment of lead-contained wastewater. Chem Eng J. 2016;290:263–72.
12. Yang C, Yu DG, Pan D, Liu XK, Wang X, Bligh SA, Williams GR. Electrospun pH-sensitive core-shell polymer nanocomposites fabricated using a tri-axial processes. Acta Biomater. 2016;35:77–86.
13. Jiang S, Duan G, Zussman E, Greiner A, Agarwal S. Highly flexible and tough concentric tri-axial polystyrene fibers. ACS Appl Mater Interfaces. 2014;6(8):5918–23.
14. Li XY, Shi CJ, Yu DG, Liao YZ, Wang X. Electrospun quercetin-loaded zein nanoribbons. Biomed Mater Eng. 2014;24(6): 2015–23.
15. Yu DG, Xu Y, Li Z, Du LP, Zhao BG, Wang X. Coaxial electrospinning with mixed solvents: from flat to round Eudragit L100 nanofibers for better colon-targeted sustained drug release profiles. J Nanomater. 2014;2014:967295.
16. Yu DG, Yang C, Jin M, Williams GR, Zou H, Wang X, Bligh SW. Medicated Janus fibers fabricated using a Teflon-coated side-by-side spinneret. Colloid Surf B. 2016;138:110–6.
17. Yang GZ, Li JJ, Yu DG, He MF, Yang JH, Williams GR. Nanosized sustained-release drug depots fabricated using modified tri-axial electrospinning. Acta Biomater. 2017;53:233–41.
18. Wang X, Li XY, Li Y, Zou H, Yu DG, Cai JS. Electrospun acetaminophen-loaded cellulose acetate nanofibers fabricated using an epoxy-coated spinneret. e-Polymers 2015;15(5):311–5.
19. Xiang Q, Ma YM, Yu DG, Jin M, Williams GR. Electrospinning using a Teflon-coated spinneret. Appl Surf Sci. 2013;284: 889–93.
20. Qian W, Yu DG, Li Y, Liao YZ, Wang X, Wang L. Dual drug release electrospun core-shell nanofibers with tunable dose in the second phase. Int J Mol Sci. 2014;15(1):774–86.
21. Yu DG, Li XY, Chian W, Li Y, Wang X. Influence of sheath solvents on the quality of ethyl cellulose nanofibers from a modified coaxial electrospinning. Biomed Mater Eng. 2014;24(1):695–701.
22. Yu DG, Li JJ, Zhang M, Williams G. High-quality Janus nanofibers prepared using three-fluid electrospinning. Chem Commun. 2017;53(33):4542–5.
23. Yan J, White K, Yu DG, Zhao XY. Sustained release multiple-component cellulose acetate nanofibers fabricated using a modified coaxial electrospinning process. J Mater Sci. 2014;49(2): 538–47.
24. Wu YH, Yu DG, Li HP, Wu XY, Li XY. Medicated structural PVP/PEG composites fabricated using coaxial electrospinning. e-Polymers 2017;17(1):39–44.
25. Xu Y, Li JJ, Yu DG, Williams GR, Yang JH, Wang X. Influence of the drug distribution in electrospun gliadin fibers on drug-release behavior. Eur J Pharm Sci. 2017;106:422–30.
26. Agarwal S, Greiner A, Wendorff JH. Electrospinning of manmade and biopolymer nanofibers – progress in techniques, materials, and applications. Adv Funct Mater. 2009;19(18):2863–79.

27. Sill TJ, Von Recum HA. Electrospinning: applications in drug delivery and tissue engineering. Biomaterials 2008;29(13):1989–2006.
28. Agarwal S, Wendorff JH, Greiner A. Use of electrospinning technique for biomedical applications. Polymer 2008;49(26):5603–21.
29. Ma ZH, Yu DG, Branford-White CJ, Zhu LM. Microencapsulation of tamoxifen: application to cotton fabric. Colloid Surface B. 2009;69(1):85–90.
30. Gamberini MC, Baraldi C, Tinti A, Palazzoli F, Ferioli V. Vibrational study of tamoxifen citrate polymorphism. J Mol Struct. 2007;840(1):29–37.
31. Siepmann J, Peppas NA. Modeling of drug release from delivery systems based on hydroxypropyl methylcellulose (HPMC). Adv Drug Delivery Rev. 2012;64:163–74.
32. Wurster DE, Taylor PW. Dissolution rates. J Pharm Sci. 1965;54:169–75.